



PII S0016-7037(02)01048-7

In situ $^{87}\text{Sr}/^{86}\text{Sr}$ investigation of igneous apatites and carbonates using laser-ablation MC-ICP-MS

MARTIN BIZZARRO,^{1*} ANTONIO SIMONETTI,¹ R. K. STEVENSON,¹ and STEPHAN KURSZAUKIS²¹GÉOTOP, Université du Québec à Montréal, Station Centre-ville, P.O. Box 8888, Montréal, PQ H3C 3P8, Canada²De Beers GeoScience Center, P.O. Box 82232, Southdale, 2135, South Africa

(Received November 13, 2001; accepted in revised form July 1, 2002)

Abstract—In situ Sr isotopic compositions of coexisting apatite and carbonate for carbonatites from the Sarfartoq alkaline complex, Greenland, have been determined by laser-ablation multicollector inductively coupled plasma mass spectrometry. This study is the first to examine the extent of Sr isotopic homogeneity among coexisting igneous minerals containing high Sr (>3000 ppm) and low Rb (<<1 ppm) contents within a single ~50- μm -thick thin-section mount. This technique is capable of producing measured $^{87}\text{Sr}/^{86}\text{Sr}$ values with analytical precision (~0.005%, 2σ) approaching those obtained by thermal ionization mass spectrometry but in a much shorter interval of time (100 s vs. >1 h, respectively). The combined total analyses ($n = 107$) of apatite and carbonate yield $^{87}\text{Sr}/^{86}\text{Sr}$ compositions ranging from ~0.7025 to ~0.7031. This relatively large variation in Sr isotopic compositions (~0.0006) is ~1 order of magnitude larger than the estimated external reproducibility (~0.00005, 2σ) of the method. The large range in $^{87}\text{Sr}/^{86}\text{Sr}$ values suggests that apatite and carbonate precipitated predominantly under nonequilibrium conditions. The isotopic variations observed within individual hand specimens may therefore reflect larger (regional) scale open-system processes, possibly involving mixing of carbonatitic melts derived from distinct mantle sources or from a common isotopically heterogeneous mantle. Copyright © 2003 Elsevier Science Ltd

1. INTRODUCTION

The Sarfartoq alkaline province is located on the southwestern coast of Greenland and consists of a 600-Ma carbonatite intrusive complex on which is centered a contemporaneous kimberlite dike swarm. The latter is interpreted as series of cone sheets dipping toward the core area of the carbonatite (Larsen and Rex, 1992). At numerous localities, the kimberlite dikes are host to peridotite xenoliths. The alkaline complex is intruded into high-grade Precambrian gneisses and straddles the boundary between the southern front of the Proterozoic Nagssuqotidian orogen and units of the Greenland Western Archean craton. The Nagssuqotidian orogen is an east-north-east trending 150-km-wide belt consisting of Archean tonalitic and granodioritic orthogneisses interleaved with Proterozoic orthogneisses and supracrustal units (Kalsbeek et al., 1987; Kalsbeek and Nutman, 1996). The Sarfartoq complex is predominantly magnesiocarbonatite, with lenses of calciocarbonatite restricted to the core area of the complex (Secher and Larsen, 1980).

Carbonatites, igneous rocks containing > 50% carbonate by volume, are ideally suited for laser-ablation (LA) studies because their constituent minerals (e.g., carbonate and apatite) are Sr-rich (>3000 ppm) and Rb-poor (<<1 ppm) phases. Moreover, carbonate and apatite are not necessarily contemporaneous liquidus phases in carbonatite magmas (Biggar, 1969); thus, they can record potential isotopic changes in a dynamic system because each retains the composition of the host magma at different times during the crystallization history of the melt (providing that reequilibration with the host melt does not

occur). Because results from melt experiments (e.g., Wallace and Green, 1988) and isotopic data (Nd, Pb, and Sr; e.g., Bell, 1998) have clearly established that carbonatitic melts are of a deep-seated mantle origin, carbonatites can provide valuable information about the composition of the different mantle sources involved in their genesis (e.g., East African Rift: Bell and Simonetti, 1996; Bell and Tilton, 2001; Deccan alkaline complexes of India: Simonetti et al., 1998; Greenland: Bizzarro et al., 2002). The scale at which the “isotope fingerprinting” of these large-scale mantle processes occurs remains unclear, and it is not known whether they can be traced by small-scale isotopic examination of different minerals within single whole-rock samples.

Over the past decade, the introduction of multicollector inductively coupled plasma mass spectrometry (MC-ICP-MS) instruments has provided the ability to measure a larger variety of stable and radiogenic isotope systems. This is attributable to their high ion transmission and flexibility for sample introduction, simultaneous detection of ion signals using analog detectors, and flat-top peaks. These features have combined to generate an instrument capable of producing isotope measurements with precision comparable to those obtained by thermal ionization mass spectrometry (TIMS). Moreover, the coupling of LA systems to MC-ICP-MS instruments has added the potential of providing spatially resolved, high-precision measurements for a variety of radiogenic isotope systems, including $^{87}\text{Sr}/^{86}\text{Sr}$ (Jackson et al., 2001, and references therein). Christensen et al. (1995) first reported the application of LA-MC-ICP-MS to Sr isotope studies and succeeded in obtaining precise and accurate measurements of modern marine gastropods and plagioclase. These experiments, which employed long ablation times (13 to 17 min), documented isotopic disequilibrium between two plagioclase grains from a Long Valley basalt that was interpreted as indicative of magma mixing.

* Author to whom correspondence should be addressed, at Geologisk Museum, Øster Voldgade 5-7, 1350 Copenhagen K, Denmark (mbi@dlc.ku.dk).

Table 1. Major element compositions of whole-rock carbonatites and average compositions of associated carbonates.

	SARF-10			SARF-03	
	Whole-rock	Calcite ($n = 15$)	Dolomite ($n = 14$)	Whole-rock	Dolomite ($n = 31$)
SiO ₂	0.60			0.03	
TiO ₂	0.01			0.01	
Al ₂ O ₃	0.17			0.02	
FeO	2.06	0.37	3.36	4.13	4.92
MnO	0.25	0.22	0.30	0.59	0.59
MgO	8.20	0.47	19.00	16.85	17.64
CaO	39.03	55.20	29.46	28.73	28.09
Na ₂ O	0.05			0.06	
K ₂ O	0.06			0.00	
P ₂ O ₅	4.71			0.11	
SrO	0.39	0.56	0.30	0.90	0.96
LOI/CO ₂	44.24	43.18	47.56	48.24	47.80
Total	99.8	100.0	100.0	99.7	100.0

Analyses reported in weight percentage.

Recently, Sr isotope stratigraphy studies of individual plagioclase phenocrysts using either microdrilling (Davidson and Tepley, 1997) or LA-MC-ICP-MS (Davidson et al., 2001) techniques have clearly indicated that equilibrium conditions were not attained with the host magma. This feature, indicative of open-system behavior, attests to the complex crystallization histories of some lavas before solidification. Moreover, it suggests that certain processes, such as wall-rock contamination and magma mixing, can modify the isotopic composition of magmas and may be common attributes of magmatic systems. Investigations of whole-rock samples make the important assumption that all constituent minerals are in isotopic equilibrium. In magma systems with complex (open-system) petrogenetic histories, therefore, whole-rock isotopic compositions would simply reflect the average, weighted value for the different minerals with distinct signatures.

We have investigated the Sr isotopic composition of individual apatite and carbonate grains for carbonatites from the Sarfartoq complex of southwestern Greenland using LA-MC-ICP-MS. Here, we document the variation in the ⁸⁷Sr/⁸⁶Sr composition of coexisting apatite and carbonate (if any) and attempt to constrain the mechanisms generating the observed variations. By comparison with the whole-rock Sr isotopic compositions of associated kimberlites and their mantle peridotite xenoliths, we evaluate the contribution of possible mantle sources involved in the genesis of the carbonatites at Sarfartoq.

2. ANALYTICAL METHODS

Whole-rock major element compositions of carbonatites were determined with a Philips PW 1400 X-ray fluorescence (XRF) spectrometer using 10 to 15 g of powdered rock (Table 1). XRF analyses of major oxides were determined from fused beads prepared from ignited samples, and Sr XRF analyses were determined from pressed pellets. Uncertainties for major (>5%) and minor (<5%) oxides are better than 2 and 5% of quoted values, respectively. The major element compositions of calcites and carbonates were determined with a JEOL 8900 superprobe (Tables 1 and 2). Microprobe analyses were conducted with an acceleration voltage of 15 Kv and beam current at 5×10^{-8} A, and the diameter was set at 5 μ m. Uncertainties for major (>5%) and minor (<5%) oxides analyzed by microprobe are better than 2 and 5% of quoted values, respectively, and 10 and 20% of quoted value for SrO and Ce₂O₃, respectively.

LA experiments were conducted on \sim 50- μ m-thick thin sections

prepared for electron microprobe work. In situ Sr isotope analyses were obtained at GEOTOP, Université du Québec à Montréal, using an MC-ICP mass spectrometer (IsoProbe, Micromass) coupled to a 193-nm (ArF) excimer laser (Compex 102, Lambda Physik) and an optics system by Merchantek–New Wave Research. The ablation was conducted under a helium atmosphere in a non-jet ablation cell at a flow rate of \sim 0.5 L/min. Helium was used to flush out the ablation cell instead of Ar because previous studies have clearly shown that the former increases instrument sensitivity because of a higher degree of sample transport efficiency and reduced deposition at the ablation site (e.g., Eggins et al., 1998; Horn et al., 2000; Fig. 1). Ar gas was mixed into the “sample-out” line from the ablation cell before arrival at the plasma via a “Y connection” to an Aridus microconcentric nebulizer. Laser pulse energies were in the range of 70 to 90 mJ (25-ns pulse duration) at a repetition rate of 1 to 2 Hz (depending on the spot size), corresponding to energy densities of \sim 4 to 5 J/cm² at the sample surface. The spot sizes used for the ablation experiments varied from 80 to 330 μ m (Fig. 1). Sr isotope data were obtained in static, multicollection mode using six Faraday collectors. For each sample, data acquisition consisted of a 50-s measurement of the gas blank before the start of ablation, a similar method to that employed by Davidson et al. (2001) for an IsoProbe MC-ICP mass spectrometer. This measurement is critical because it monitors ⁸⁶Kr, which interferes with the ⁸⁶Sr signal. The isobaric interference of ⁸⁷Rb was monitored by measuring the ⁸⁵Rb ion signal (e.g., Table 3). Using Rb-doped synthetic glass standards, Davidson et al. (2001) investigated the relationship between the Rb/Sr ratio in feldspars and their measured ⁸⁷Sr/⁸⁶Sr values obtained during LA. The results indicated that for Rb-doped standards with Rb/Sr ratios of \sim 0.0015, the ⁸⁷Sr/⁸⁶Sr values obtained by LA were \sim 0.0001 higher compared to those obtained by TIMS analysis for the same standards. The Rb/Sr values for the majority of the carbonate and apatite grains investigated here (Table 3), however, are much < 0.0015 (*average* = 0.00004, $n = 107$), and therefore, the ⁸⁷Rb interference on the measured ⁸⁷Sr/⁸⁶Sr is considered negligible. In the extreme case, it is approximately the same magnitude as the typical 2σ internal precision (\sim 0.00005) associated with the ⁸⁷Sr/⁸⁶Sr value for individual LA analyses. The effectiveness of the combined interference corrections (i.e., Kr, Rb) applied to the analyses can be directly evaluated by monitoring the invariant ⁸⁴Sr/⁸⁸Sr (0.00675) and ⁸⁴Sr/⁸⁶Sr (0.0565) values, and these are listed in Table 3. It is extremely important to carefully monitor these invariant ratios because the presence of either doubly charged middle to heavy rare earth elements (masses 144 to 176 divided by $Z = 2^+$), molecular species from Ca (⁴²Ca₂, ⁴³Ca₂, ⁴⁴Ca₂), or oxides of Fe (⁵⁴Fe or ⁵⁶Fe + 2[¹⁶O]) formed during the ablation process would create isobaric interferences within the mass range used for Sr isotope data acquisition. Ion beam intensities for most samples varied from \sim 2 to 5×10^{-11} A of ⁸⁸Sr. Time-resolved analysis for the ablation runs was not needed because of the simultaneous acquisition of the ion signals (multicollection) and the relative stability of the ion

Table 2. Major element variation among single apatite crystals.

Spot #	F	Na ₂ O	P ₂ O ₅	CaO	Ce ₂ O ₃	SrO	SO ₃	FeO	Total
Apatite 1									
1	2.24	0.17	41.82	54.34	0.31	0.48	0.02	0.07	99.45
2	2.37	0.24	41.62	54.18	0.18	0.51	0.05	0.07	99.21
3	2.21	0.24	41.36	54.12	0.13	0.49	0.03	0.09	98.67
4	2.19	0.22	41.62	54.36	0.17	0.46	0.05	0.08	99.15
5	2.15	0.25	41.42	54.10	0.13	0.51	0.03	0.06	98.65
6	2.46	0.18	41.80	54.38	0.14	0.54	0.02	0.04	99.56
7	2.13	0.23	41.31	54.29	0.15	0.48	0.04	0.08	98.72
8	2.15	0.24	41.45	54.07	0.20	0.50	0.05	0.10	98.75
9	2.16	0.22	41.66	53.92	0.13	0.53	0.04	0.09	98.74
10	2.14	0.18	41.12	54.39	0.17	0.59	0.04	0.06	98.68
11	2.04	0.24	41.66	53.50	0.20	0.51	0.04	0.08	98.26
12	2.33	0.23	41.66	54.18	0.15	0.50	0.07	0.09	99.20
Apatite 2									
1	2.33	0.24	41.42	54.05	0.15	0.46	0.06	0.11	98.80
2	2.45	0.17	41.36	54.38	0.16	0.49	0.04	0.06	98.16
3	2.58	0.13	41.69	54.15	0.18	0.46	0.00	0.03	98.34
4	3.15	0.14	41.30	53.99	0.21	0.52	0.02	0.03	98.26
5	2.63	0.14	41.65	54.44	0.19	0.54	0.01	0.07	98.74
6	2.54	0.13	41.64	54.16	0.21	0.49	0.02	0.03	98.38
7	2.47	0.15	41.69	54.19	0.22	0.49	0.00	0.06	98.28
Apatite 3									
1	2.22	0.24	41.23	54.19	0.16	0.44	0.05	0.11	98.65
2	2.17	0.24	41.75	54.03	0.17	0.47	0.05	0.09	98.96
3	2.33	0.17	41.65	54.36	0.24	0.54	0.02	0.05	99.36
4	2.17	0.20	41.37	54.18	0.27	0.54	0.03	0.10	98.84

Analyses reported in weight percentage. Apatite 1 is 6.5 mm long and 2.5 mm wide, apatite 2 is 3 mm long and 1.2 mm wide, and apatite 3 is 2.1 mm long and 1 mm wide. Analyses were distributed homogeneously along the length of the crystals. All apatites are characterized by textural disequilibrium features (e.g., Fig. 3).

signals (average error $\sim 2\%$), resulting in high in-run precision (Table 3). Subsequent to the start of LA, two half-mass unit baseline measurements were obtained for each Faraday collector (within the mass range of 82.5 to 88.5), followed by ion signal measurements of 100-s intervals (50 integrations of 2 s each). The measured Sr isotope ratios were normalized to $^{84}\text{Sr}/^{86}\text{Sr} = 0.1194$ and corrected for instrumental mass bias using the exponential law (Russell et al., 1978).

Sr isotopic ratios obtained for repeated analyses of a 100-ppb solution of National Bureau of Standards (NBS) 987 ($n = 5$) for the analytical sessions in which both solution mode and LA analyses were carried out yield the following values (2σ uncertainties): $^{87}\text{Sr}/^{86}\text{Sr} = 0.71025 \pm 7$, $^{84}\text{Sr}/^{86}\text{Sr} = 0.05659 \pm 29$, and $^{84}\text{Sr}/^{88}\text{Sr} = 0.006758 \pm 34$. These are well within the accepted Sr isotopic composition for this standard, thus validating the Sr isotope data obtained in solution mode.

Samples selected for whole-rock Sr isotopic analysis by TIMS were dissolved in a mixture of HF-HCl-HNO₃ in Savillex beakers for 48 h. Sr separation was achieved by standard cation exchange chromatography, and Sr was subsequently loaded onto a single filament (Re) with a HCl-HNO₃-TaO solution for analysis using a VG-54 Sector multi-collector mass spectrometer. Analyses were obtained in static, multi-collection mode, and during the period of this study, repeated analysis of the NBS 987 standard yielded an average $^{87}\text{Sr}/^{86}\text{Sr}$ value of 0.71024 ± 4 (2σ standard deviation, $n = 10$, normalized to $^{84}\text{Sr}/^{86}\text{Sr} = 0.1194$). This $^{87}\text{Sr}/^{86}\text{Sr}$ value is identical to that obtained in solution-mode MC-ICP-MS analysis.

3. RESULTS

3.1. Mineral Chemistry

The calciocarbonatites, which were selected for the LA work (Table 1), consist of calcite and dolomite with subordinate amounts of apatite, phlogopite, magnetite, and ilmenite, and accessory phases include richterite-arfvedsonite, pyrochlore,

pyrite, and zircon (Secher and Larsen, 1980). Mineral segregation textures are evidenced by clusters of apatite or bands of large carbonate crystals associated with Fe oxide minerals (Fig. 2A). Apatite crystals ranging in size from 0.1 mm to 0.5 cm demonstrate a wide range of petrographic habits, from euhedral to irregular morphologies. Large apatite crystals often show textural disequilibrium features such as resorption and embayment (Fig. 3). A number of electron microprobe traverses were conducted along large apatite crystals exhibiting textural disequilibrium features to investigate the extent of chemical zoning. Results indicate that the major and trace (Sr, Ce) element composition of apatite is homogeneous, with no systematic variation between cores and rims (Table 2). Moreover, image analyses, including back-scattered electron (Figs. 3a and 3c) and cathodoluminescence (not shown), on a number of apatite crystals selected for LA work do not reveal any evidence of trace element zoning. Carbonate crystals exhibit a wide range of grain sizes, with the predominant texture being large crystals (2 to 10 mm) set in a fine-grained interstitial matrix (< 1 mm; Fig. 2B).

3.2. In Situ Sr Isotope Analysis: External Reproducibility

A sample of modern-day coral from the "ribbon-reef" deposit surrounding Mayotte Island in the Indian Ocean (latitude 12°50'S, longitude 45°20'E; Colonna, 1994) yielding a U-Th age of 4663 ± 80 yr (B. Ghaleb, personal communication) was investigated for its Sr isotopic composition to determine the external reproducibility (2σ) of the methodology employed in

Table 3. Sr isotopic ratios measured by laser-ablation multicollector inductively coupled plasma mass spectrometry for SARF-10 apatites and carbonates.

Analysis #	Pit size (μm)	$^{87}\text{Sr}/^{86}\text{Sr}$	$^{84}\text{Sr}/^{88}\text{Sr}$	$^{84}\text{Sr}/^{86}\text{Sr}$	^{88}Sr (V)	^{85}Rb (10^{-3}V)
Apatites						
1	330	0.70291 (05)	0.00677 (1)	0.05669 (11)	3.21	0.00
2	330	0.70289 (04)	0.00675 (1)	0.05650 (06)	4.85	0.00
3	330	0.70289 (04)	0.00677 (1)	0.05670 (06)	5.1	0.01
4	330	0.70290 (03)	0.00674 (1)	0.05644 (05)	4.92	0.01
5	330	0.70287 (03)	0.00676 (1)	0.05663 (05)	4.9	0.00
6	330	0.70288 (02)	0.00678 (1)	0.05676 (06)	4.98	0.00
7	330	0.70288 (03)	0.00677 (1)	0.05674 (05)	5.02	0.21
8	330	0.70288 (04)	0.00676 (1)	0.05663 (06)	4.91	0.00
9	330	0.70281 (03)	0.00677 (7)	0.05673 (06)	5.07	0.02
10	150	0.70273 (04)	0.00679 (1)	0.05683 (06)	4.9	0.01
11	150	0.70285 (04)	0.00673 (1)	0.05640 (08)	4.9	0.12
12	150	0.70277 (04)	0.00680 (1)	0.05694 (06)	4.9	0.01
13	150	0.70287 (08)	0.00674 (1)	0.05645 (12)	4.56	0.10
14	150	0.70278 (05)	0.00678 (1)	0.05680 (09)	4.86	0.06
15	150	0.70283 (05)	0.00678 (1)	0.05675 (09)	4.49	0.08
16	150	0.70289 (04)	0.00676 (1)	0.05659 (07)	4.2	0.49
17	150	0.70289 (05)	0.00671 (1)	0.05623 (10)	4	0.07
18	330	0.70284 (08)	0.00670 (3)	0.05609 (26)	1.12	0.00
19	330	0.70297 (10)	0.00676 (4)	0.05669 (35)	0.74	0.00
20	330	0.70281 (11)	0.00680 (3)	0.05694 (24)	1.26	0.00
21	330	0.70281 (10)	0.00670 (3)	0.05611 (25)	1.25	0.00
22	330	0.70304 (09)	0.00670 (3)	0.05609 (25)	1.31	0.00
23	330	0.70304 (16)	0.00674 (4)	0.05644 (33)	0.74	0.96
24	330	0.70292 (08)	0.00671 (2)	0.05619 (18)	1.6	0.06
25	330	0.70284 (04)	0.00671 (1)	0.05622 (11)	3.62	0.02
26	330	0.70278 (07)	0.00672 (1)	0.05630 (10)	3.12	0.00
27	330	0.70291 (05)	0.00670 (1)	0.05607 (11)	2.77	0.13
28	150	0.70252 (18)	0.00674 (5)	0.05643 (44)	0.72	0.01
29	330	0.70317 (10)	0.00678 (2)	0.05680 (20)	1.85	0.84
30	330	0.70289 (08)	0.00679 (2)	0.05689 (17)	1.92	0.08
31	330	0.70284 (08)	0.00680 (2)	0.05694 (18)	1.79	0.00
32	330	0.70280 (15)	0.00676 (2)	0.05663 (17)	1.58	0.00
33	330	0.70280 (13)	0.00680 (2)	0.05693 (20)	1.52	0.01
34	330	0.70264 (08)	0.00679 (2)	0.05690 (18)	1.65	0.05
35	330	0.70269 (08)	0.00677 (2)	0.05666 (16)	1.69	0.04
36	330	0.70268 (13)	0.00677 (2)	0.05672 (16)	1.63	0.00
37	330	0.70267 (14)	0.00679 (2)	0.05684 (16)	1.66	0.02
38	330	0.70304 (13)	0.00670 (2)	0.05614 (17)	1.67	0.00
39	330	0.70279 (09)	0.00675 (2)	0.05655 (18)	1.54	0.00
40	330	0.70262 (10)	0.00675 (3)	0.05655 (21)	1.56	0.03
41	150	0.70284 (04)	0.00673 (1)	0.05636 (06)	4.78	0.09
42	150	0.70297 (05)	0.00666 (1)	0.05579 (07)	4.58	0.08
43	150	0.70279 (05)	0.00672 (1)	0.05629 (080)	4.76	0.10
44	150	0.70282 (03)	0.00674 (1)	0.05643 (05)	4.59	0.05
45	150	0.70287 (03)	0.00671 (1)	0.05623 (07)	4.66	0.08
46	330	0.70297 (05)	0.00673 (1)	0.05640 (06)	5.72	0.07
47	330	0.70294 (04)	0.00677 (1)	0.05672 (07)	5.52	0.03
Averages		0.70285 (24)	0.00675 (7)	0.05654 (28)	3.25	0.08
Coarse-grained carbonates						
1	330	0.70297 (06)	0.00669 (2)	0.05600 (14)	2.26	0.00
2	330	0.70269 (05)	0.00674 (1)	0.05644 (04)	3.42	0.08
3	330	0.70277 (11)	0.00676 (3)	0.05658 (24)	1.17	0.01
4	330	0.70266 (03)	0.00677 (1)	0.05671 (05)	5.78	0.01
5	330	0.70298 (10)	0.00671 (4)	0.05618 (29)	1.05	0.15
6	330	0.70291 (06)	0.00671 (7)	0.05616 (62)	0.48	0.00
7	100	0.70283 (04)	0.00676 (1)	0.05660 (05)	6.99	0.14
8	330	0.70291 (11)	0.00679 (1)	0.05687 (06)	6.64	0.00
9	150	0.70277 (05)	0.00675 (1)	0.05653 (06)	6.92	0.26
10	330	0.70281 (04)	0.00679 (1)	0.05688 (06)	3.64	0.07
11	150	0.70289 (04)	0.00673 (1)	0.05638 (06)	4.87	0.01
12	330	0.70254 (03)	0.00676 (1)	0.05659 (06)	4.16	0.02
13	150	0.70292 (02)	0.00671 (1)	0.05622 (06)	4.71	0.03
14	330	0.70283 (07)	0.00675 (2)	0.05649 (17)	1.51	0.01
15	330	0.70287 (04)	0.00677 (1)	0.05671 (07)	3.84	0.06
16	330	0.70300 (08)	0.00675 (2)	0.05655 (16)	1.55	0.06
17	330	0.70261 (03)	0.00678 (1)	0.05676 (07)	4.11	0.13

(continued)

Table 3. (Continued)

Analysis #	Pit size (μm)	$^{87}\text{Sr}/^{86}\text{Sr}$	$^{84}\text{Sr}/^{88}\text{Sr}$	$^{84}\text{Sr}/^{86}\text{Sr}$	^{88}Sr (V)	^{85}Rb (10^{-3}V)
18	330	0.70263 (03)	0.00675 (1)	0.05691 (07)	3.87	0.04
19	330	0.70260 (04)	0.00680 (1)	0.05694 (08)	3.85	0.02
20	150	0.70281 (04)	0.00676 (1)	0.05664 (08)	4.23	0.02
21	330	0.70284 (04)	0.00675 (1)	0.05655 (08)	3.73	0.06
22	150	0.70289 (05)	0.00673 (1)	0.05634 (08)	3.09	0.09
23	150	0.70286 (03)	0.00675 (1)	0.05649 (08)	4.70	0.04
24	330	0.70283 (05)	0.00678 (1)	0.05676 (08)	3.44	0.07
25	150	0.70282 (04)	0.00675 (1)	0.05655 (08)	4.70	0.00
26	330	0.70269 (04)	0.00680 (1)	0.05697 (08)	3.28	0.12
27	330	0.70282 (04)	0.00670 (1)	0.05611 (08)	3.40	0.05
28	330	0.70277 (05)	0.00678 (1)	0.05680 (08)	3.34	0.08
29	150	0.70286 (03)	0.00677 (1)	0.05667 (08)	4.72	0.10
30	330	0.70253 (05)	0.00676 (1)	0.05663 (08)	3.84	0.05
31	150	0.70282 (03)	0.00679 (1)	0.05683 (08)	4.50	0.21
32	330	0.70275 (06)	0.00679 (1)	0.05689 (08)	3.44	0.10
33	330	0.70273 (06)	0.00679 (1)	0.05683 (08)	3.61	0.06
34	330	0.70254 (04)	0.00678 (1)	0.05678 (09)	4.22	0.23
35	330	0.70283 (04)	0.00676 (1)	0.05658 (09)	3.38	0.11
36	150	0.70276 (04)	0.00671 (1)	0.05623 (09)	2.70	0.10
37	330	0.70279 (04)	0.00679 (1)	0.05684 (09)	4.50	0.00
38	150	0.70286 (04)	0.00676 (1)	0.05661 (09)	4.66	0.07
39	330	0.70284 (04)	0.00680 (1)	0.05691 (10)	3.60	0.08
40	330	0.70285 (04)	0.00675 (1)	0.05655 (10)	4.64	0.04
41	330	0.70284 (08)	0.00680 (1)	0.05691 (10)	3.44	0.00
42	150	0.70265 (06)	0.00679 (1)	0.05685 (10)	2.51	0.00
43	330	0.70259 (04)	0.00674 (1)	0.05642 (10)	3.70	0.08
44	150	0.70281 (04)	0.00676 (3)	0.05658 (11)	8.77	0.30
45	150	0.70278 (05)	0.00678 (1)	0.05678 (11)	2.58	0.01
46	150	0.70280 (04)	0.00675 (1)	0.05656 (11)	2.52	0.00
47	330	0.70278 (02)	0.00676 (1)	0.05662 (11)	7.37	0.10
48	150	0.70282 (05)	0.00670 (1)	0.05613 (11)	2.50	0.87
49	330	0.70291 (05)	0.00673 (1)	0.05637 (11)	7.13	0.19
50	330	0.70289 (04)	0.00676 (1)	0.05662 (11)	7.39	0.23
51	150	0.70282 (04)	0.00675 (1)	0.05653 (12)	4.83	0.30
52	150	0.70276 (06)	0.00671 (2)	0.05622 (13)	2.31	0.08
53	150	0.70294 (05)	0.00672 (2)	0.05622 (13)	2.45	0.00
54	330	0.70285 (09)	0.00673 (8)	0.05634 (67)	0.45	0.03
55	100	0.70282 (05)	0.00679 (2)	0.05684 (14)	3.19	0.03
Fine-grained carbonates						
56	330	0.70289 (05)	0.00671 (1)	0.05623 (05)	5.47	0.02
57	330	0.70282 (04)	0.00677 (1)	0.05670 (05)	5.83	0.01
58	330	0.70290 (04)	0.00674 (1)	0.05645 (05)	5.18	0.04
59	330	0.70295 (04)	0.00676 (1)	0.05665 (07)	5.41	0.01
60	330	0.70288 (05)	0.00676 (1)	0.05660 (07)	5.10	0.01
Averages		0.70280 (22)	0.00676 (6)	0.05658 (49)	4.01	0.08

Numbers in parentheses correspond to analytical uncertainties in the last decimal place and are quoted at the 2σ level. (V) = volt: 1×10^{-11} A ion signal intensity.

this study. The LA experiments were conducted over 2 consecutive days, and repeated measurements ($n = 30$) using an $80\text{-}\mu\text{m}$ spot size yielded an average $^{87}\text{Sr}/^{86}\text{Sr}$ value of 0.709097 ± 0.000047 (2σ standard deviation), with corresponding average $^{84}\text{Sr}/^{86}\text{Sr}$ and $^{84}\text{Sr}/^{88}\text{Sr}$ ratios of 0.00672 ± 0.00004 (2σ standard deviation) and 0.0562 ± 0.0003 (2σ standard deviation), respectively (Fig. 4A). Of interest, the 2σ external reproducibility obtained for the sample of coral is almost identical to the average 2σ internal precisions of ± 0.00005 and ± 0.00007 for the carbonate and apatite, respectively (as calculated from uncertainties listed in Table 3). The accuracy of the LA results was investigated by obtaining TIMS measurements on four separate fragments of the coral. These four fragments, weighing ~ 0.050 g each, were dissolved, and Sr was separated using conventional cation exchange chromatography. The Sr isotopic results obtained by TIMS are listed in Table 4 and yield an

average $^{87}\text{Sr}/^{86}\text{Sr}$ value of 0.709098 ± 0.000019 (2σ standard deviation). The latter is identical to the average Sr isotopic composition based on the LA runs and thus provides strong evidence for the accuracy of the results obtained in this study.

For comparison, a mollusk sample from a terrace deposit located at Esmeraldas (northwestern Ecuador) yields a U-Th date of $\sim 55,000$ yr; however, the accurate stratigraphic age for the terrace deposit is $\sim 125,000$ yr (B. Ghaleb, personal communication). This feature was attributed to postdepositional, open-system behavior suffered by the mollusk. Figure 4B illustrates the measured $^{87}\text{Sr}/^{86}\text{Sr}$ values obtained for 35 analyses of the mollusk over the period of this study. The average $^{87}\text{Sr}/^{86}\text{Sr}$ value is 0.70901 ± 0.0001 (2σ standard deviation), and the average $^{84}\text{Sr}/^{86}\text{Sr}$ and $^{84}\text{Sr}/^{88}\text{Sr}$ ratios obtained are 0.0567 ± 0.0004 (2σ) and 0.00677 ± 0.00008 (2σ), respectively. In contrast to the LA results from the coral, the external

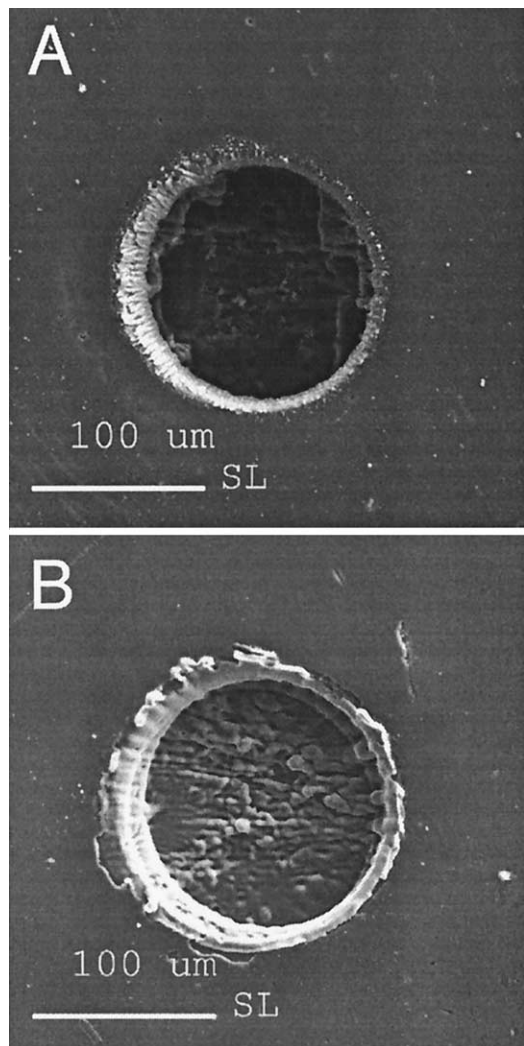


Fig. 1. Scanning electron microscope images of laser-ablation (LA) pits. (A) 150- μm pit in carbonate. (B) 150- μm pit in apatite. LA experiments were conducted in He atmosphere (0.450 L/min) at a repetition rate of 1 to 2 Hz and a laser pulse energy of ~ 90 mJ (at 22 Kv), corresponding to energy densities of ~ 5 J/cm 2 . Note the absence of accumulated ablated particles surrounding the pits.

reproducibility (2σ , ± 0.0001) for the Sr isotopic measurements of the mollusk is twice as large and roughly double the average internal precision for the individual ablation analyses (Fig. 4B). Thus, the large-scale isotopic homogeneity of the mollusk was investigated using two sample fragments (0.050 and 0.130 g) taken randomly from the piece complementary (i.e., the other half) to the one used for the LA experiment. These were dissolved and then processed through conventional cation exchange chromatography and analyzed using solution-mode MC-ICP-MS. The Sr isotopic ratios for the two fragments (also shown in Fig. 4B) exhibit a certain degree of isotopic heterogeneity and essentially bracket the results for the individual LA analyses. Thus, the distribution of the LA data for the mollusk is not entirely instrument induced but simply reflects the inherent isotopic heterogeneity of the sample. In summary, the LA Sr isotopic values obtained for both the samples of coral and mollusk indicate the effectiveness of the technique in detecting

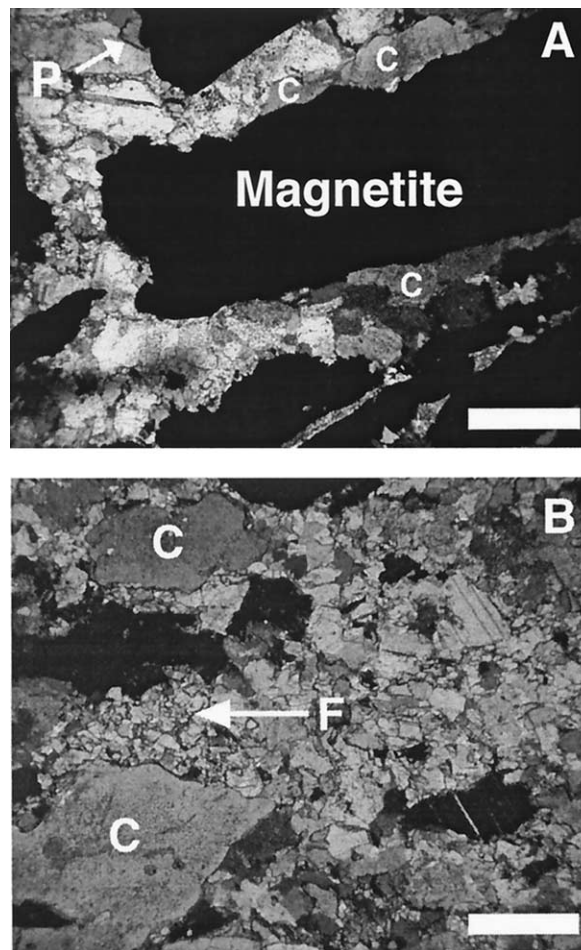


Fig. 2. Microphotographs taken under polarized light of textural features observed in sample SARF-10. Scale bars represent 2 mm. (A) Coarse carbonate (C) crystals associated with magnetite. Phlogopite inclusions (P) are generally restricted to the carbonate crystals associated with the magnetite. (B) Coarse carbonate (C) crystals set in a finer carbonate (F) matrix.

isotopic heterogeneity within a single sample at the millimeter scale.

The values obtained for the $^{84}\text{Sr}/^{86}\text{Sr}$ and $^{84}\text{Sr}/^{88}\text{Sr}$ measurements for both the coral and mollusk samples are within error of the accepted reference values (0.0565 and 0.00675, respectively), thus validating the methodology and proving the effectiveness of the correction for the gas blank (i.e., ^{86}Kr). For sample SARF-03, however, the measured $^{87}\text{Sr}/^{86}\text{Sr}$ compositions are clearly correlated with the $^{84}\text{Sr}/^{86}\text{Sr}$ values (Fig. 5A), indicating that the variations in the former are an analytical artifact. This is clearly not the case for sample SARF-10 (Fig. 5B), therefore suggesting that this contrasting behavior is related to a significant difference in the major element composition of the SARF-03 carbonates. The major element compositions of samples SARF-03 and SARF-10 are listed in Table 1, and one significant difference is the higher Fe content in the former compared to the latter (4.13 vs. 2.06 wt.%, respectively). It is possible that isobaric interferences on masses 86 and 88 related to Fe oxides produced during the LA result in

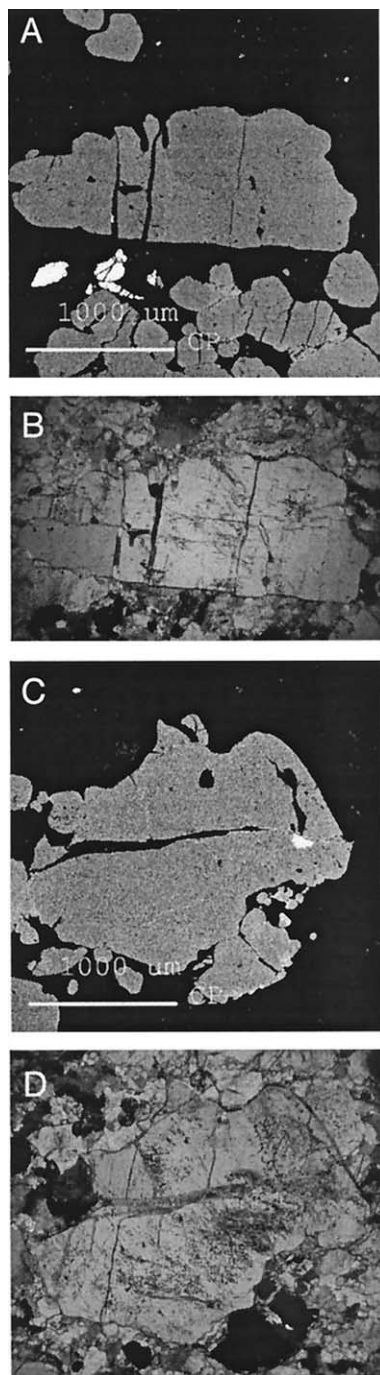


Fig. 3. (A and C) Back-scattered electron images and (B and D) microphotographs taken under polarized light of anhedral apatite crystals from sample SARF-10. Note embayment, resorption features, and lack of internal chemical zoning in both apatite grains.

erroneous corrections of the mass bias (using $^{86}\text{Sr}/^{88}\text{Sr} = 0.1194$), which in turn yield inaccurate $^{87}\text{Sr}/^{86}\text{Sr}$ values.

To more accurately assess this hypothesis, a series of LA experiments were conducted with the assistance of back-scattered electron imaging and electron microprobe analysis to clearly distinguish between dolomite and calcite grains (Fig. 6A). The results of 13 LA analyses of dolomite grains in an

area (2.5 mm^2) of sample SARF-10 are plotted in a diagram of $^{84}\text{Sr}/^{86}\text{Sr}$ vs. $^{87}\text{Sr}/^{86}\text{Sr}$ (Figs. 6b and 6c). The results clearly show once again a significant correlation between these two ratios for the dolomites ($y = -4.9577x + 3.5403$, $r^2 = 0.78$; Fig. 6C), whereas a similar plot (not shown) for analyses of neighboring calcite grains ($n = 6$) is completely scattered. A best-fit regression of the data shown in Figure 5A for sample SARF-03 yields a slope of -4.4 ± 1.3 (y intercept = 3.15 ± 0.93 , $MSWD = 7.7$, 95% confidence level), similar to the result obtained for the dolomites from sample SARF-10 (-5.7 ± 1.9 , y intercept = 4.1 ± 1.3 , $MSWD = 53$, 95% confidence level; Fig. 6C). This feature suggests that the artificial correlations noted in both samples may be controlled by the same parameter (i.e., molecular interference). The higher $^{84}\text{Sr}/^{86}\text{Sr}$ values for the SARF-03 carbonates (Fig. 5A) compared to those for the dolomites ablated in SARF-10 (Fig. 6A) may be attributed to their higher average FeO content (4.9 vs. 3.4 wt.%, respectively; Table 1). Lastly, the Sr isotopic results for the dolomites (Fig. 6C) indicate that the analyses closest to the accepted $^{84}\text{Sr}/^{86}\text{Sr}$ value (i.e., 0.0565) are characterized by the least radiogenic $^{87}\text{Sr}/^{86}\text{Sr}$ composition (<0.7027).

3.3. In Situ Sr Isotope Analyses: Magmatic Carbonate and Apatite

LA-MC-ICP-MS results for carbonates and apatites are listed in Table 3. Reconnaissance analyses were conducted principally on cores of apatite and carbonate crystals for five different thin sections from sample SARF-10. Forty-seven in situ analyses of apatites, using spot sizes ranging from 150 to 330 μm , yield a large range of $^{87}\text{Sr}/^{86}\text{Sr}$ values for all sections, i.e., from 0.70252 to 0.70317. Similarly, 60 analyses of carbonate from the five different thin sections yielded a range of values between 0.70253 and 0.70300 (Fig. 7). The observed spread in $^{87}\text{Sr}/^{86}\text{Sr}$ ratios overlaps the average TIMS whole-rock value of 0.70279 ± 4 (2σ standard deviation, $n = 5$) for this sample. A number of whole-rock powder samples were leached to assess the possible extent of isotopic heterogeneity due to the presence of low-temperature subsolidus phases of distinct isotopic composition. Seven HCl leachates (carbonate fraction) from samples representing different parts of the outcrop area (25 m^2) were analyzed by TIMS and yielded Sr isotope compositions between 0.70276 and 0.70284 ($average = 0.70280 \pm 4$, $n = 7$). The range defined by TIMS analyses does not bracket the peak observed in the both the carbonate and apatite distributions but is slightly offset to less radiogenic compositions (Fig. 8). Although no correlation exists between ^{88}Sr ion signal intensity (i.e., Sr abundance) and isotopic composition, the offset in the histogram distribution suggests that carbonate and apatite grains containing the least radiogenic Sr isotope compositions have the highest strontium content. Contrarily, the average $^{87}\text{Sr}/^{86}\text{Sr}$ compositions calculated for both apatite and carbonate using the individual LA runs (0.70284 and 0.70280, respectively; Table 3) are identical to each other (within error) and to the whole-rock Sr isotope values obtained by TIMS analysis (0.70279).

There is some evidence to suggest that the Sr isotopic composition does correlate with the petrographic textures of the carbonate crystals. Five analyses of fine-grained interstitial

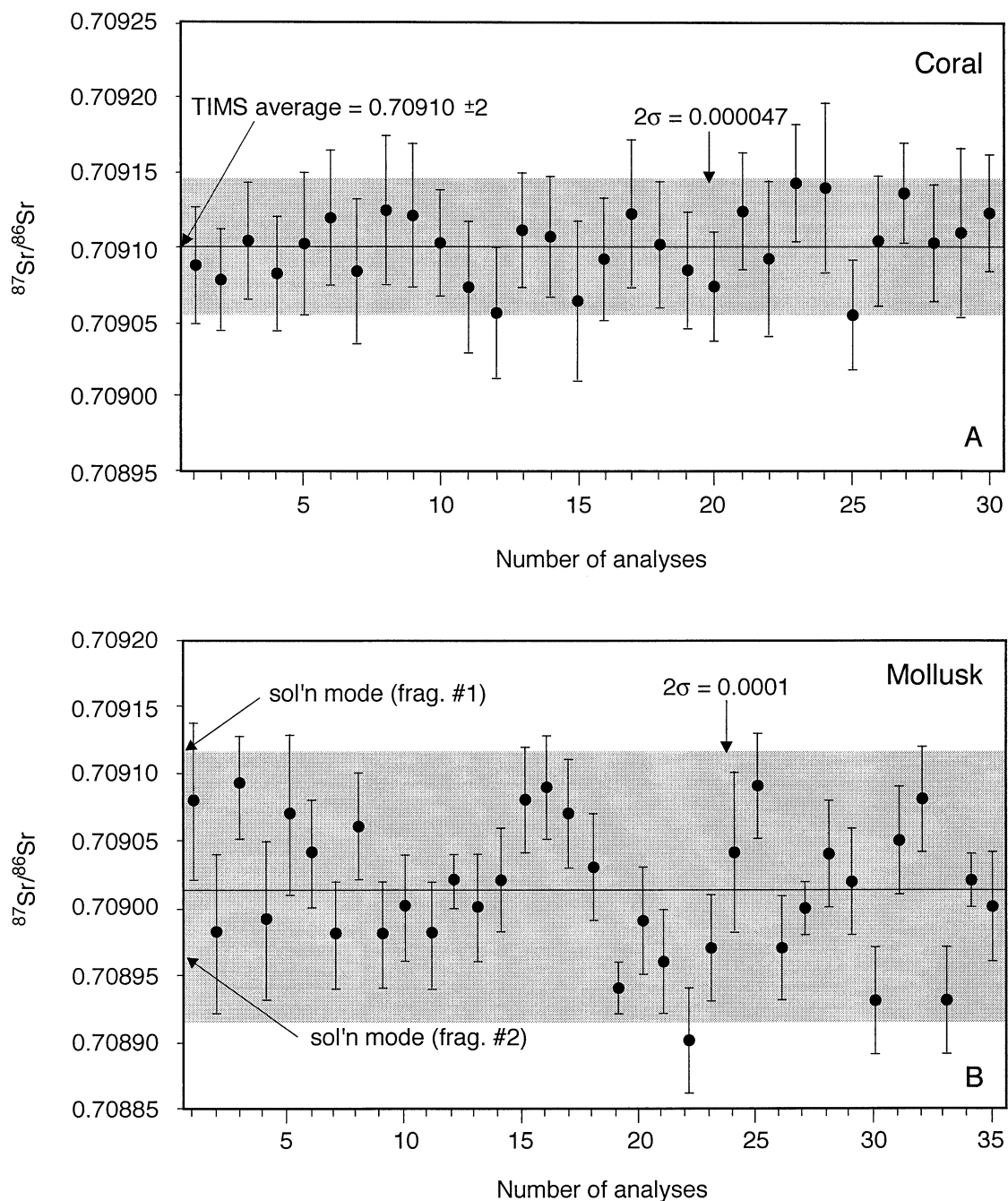


Fig. 4. Individual $^{87}\text{Sr}/^{86}\text{Sr}$ isotope analyses for the (A) “in-house” coral and (B) mollusk standards using laser-ablation multicollector inductively coupled plasma mass spectrometry (MC-ICP-MS). The Sr isotopic compositions determined using solution-mode MC-ICP-MS analysis for two separate mollusk fragments are also shown for comparison (B). Gray bands in both diagrams represent 2σ -level external reproducibility.

carbonate (e.g., Fig. 2B) yielded radiogenic compositions (0.70289 ± 8) compared to the range defined by the larger crystals (0.7026 to 0.7030). In addition, the least radiogenic isotopic compositions are typically recorded by carbonate in close association with magnetite crystals and are also characterized by the presence of zoned phlogopite inclusions (Fig. 2A). The latter are generally absent in the large carbonate crystals, which are ubiquitous throughout the sections. Core-

Table 4. Sr isotopic ratios of coral standard determined by thermal ionization mass spectrometry.

Sample number	$^{87}\text{Sr}/^{86}\text{Sr}$	2σ	$^{84}\text{Sr}/^{88}\text{Sr}$	$^{84}\text{Sr}/^{86}\text{Sr}$
1	0.709107	0.000020	0.006745	0.056489
2	0.709106	0.000017	0.006744	0.056471
3	0.709093	0.000014	0.006746	0.056495
4	0.709084	0.000016	0.006744	0.056478
Average	0.709098	0.000020	0.006744	0.056483

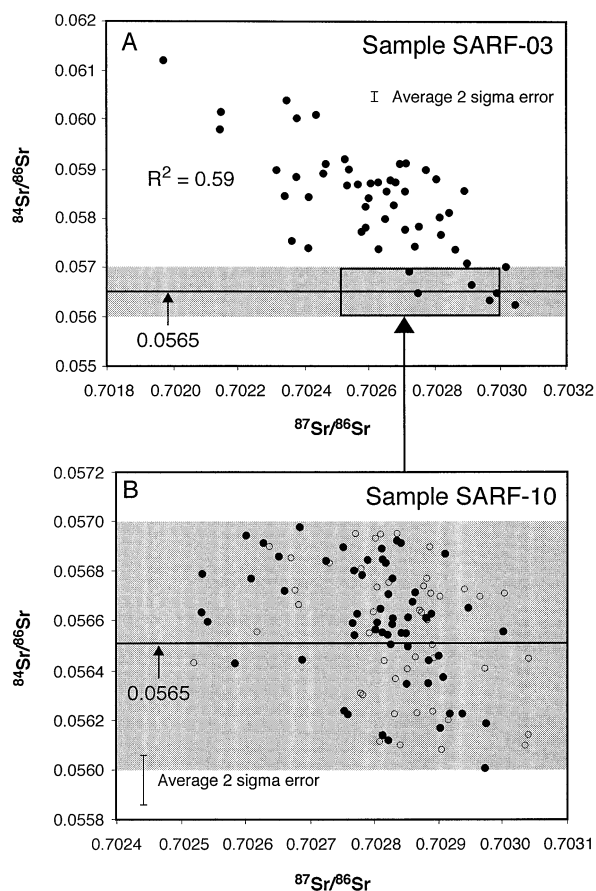


Fig. 5. Correlation diagrams of $^{84}\text{Sr}/^{86}\text{Sr}$ vs. $^{87}\text{Sr}/^{86}\text{Sr}$. Solid circles = carbonate analyses, open circles = apatite analyses. The accepted $^{84}\text{Sr}/^{86}\text{Sr}$ value is 0.0565. (A) Sample SARF-03 displays a negative correlation between $^{87}\text{Sr}/^{86}\text{Sr}$ and $^{84}\text{Sr}/^{86}\text{Sr}$ values. Box outlines range for data obtained from sample SARF-10. (B) Sample SARF-10. Note lack of correlation for both apatites and carbonates crystals and clustering of data around the accepted $^{84}\text{Sr}/^{86}\text{Sr}$ value of 0.0565.

rim analyses of the micas reveal that they are characterized by an increase in Fe and decreases in both Al and, to a lesser extent, Si contents (Table 5). These compositional trends are typical of crystallization in the presence of magnetite, which forms during the latter stages of the solidification history of carbonate magmas, driving the composition of the micas toward tetraferriphlogopite (McCormick and Le Bas, 1996). Thus, it is likely that the phlogopite-bearing carbonate crystals with relatively unradiogenic Sr isotopic compositions formed during the late stages of the crystallization history of the melt.

Potential isotopic heterogeneity within individual apatite crystals was investigated by conducting traverses across several relatively large apatite grains. The $^{87}\text{Sr}/^{86}\text{Sr}$ compositions measured across these two traverses show negligible isotopic variations (Fig. 9) and are thus considered to be in isotopic equilibrium. The traverses illustrated in Figure 9 indicate that one apatite grain records slightly more radiogenic Sr isotopic compositions than the range outlined by TIMS, whereas the other grain is characterized by values that are within the TIMS analyses.

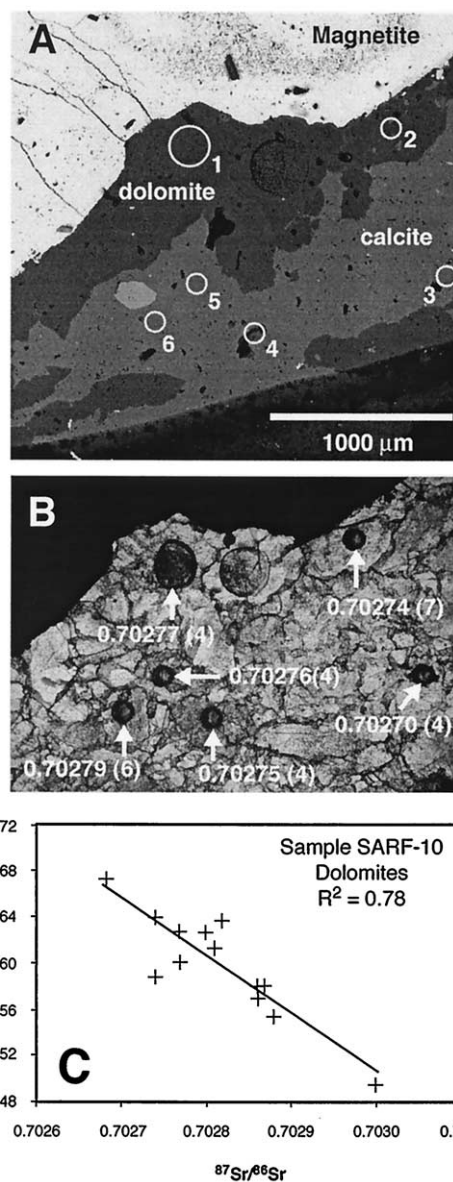


Fig. 6. (A) Back-scattered electron image and (B) microphotographs taken under transmitted light showing spatial relationships between dolomite, calcite, and magnetite crystals, and location of laser-ablation pits with corresponding Sr isotopic composition. (C) Correlation diagram of $^{84}\text{Sr}/^{86}\text{Sr}$ vs. $^{87}\text{Sr}/^{86}\text{Sr}$ for dolomite grains shown in (A). Pit sizes are 330 μm for number 1 and 80 μm for numbers 2 to 6.

4. DISCUSSION

4.1. Isotopic Disequilibria

LA-MC-ICP-MS data for the apatite and carbonate crystals strongly suggest that these minerals precipitated under non-equilibrium conditions. The large spread in Sr isotopic ratios recorded by these minerals indicates that the melt was undergoing extensive isotopic change during crystallization. In addition, the apatites and carbonates define a similar spread in Sr isotopic ratios (Figs. 7 and 8). This feature suggests that crystallization of apatite and carbonate occurred concurrently

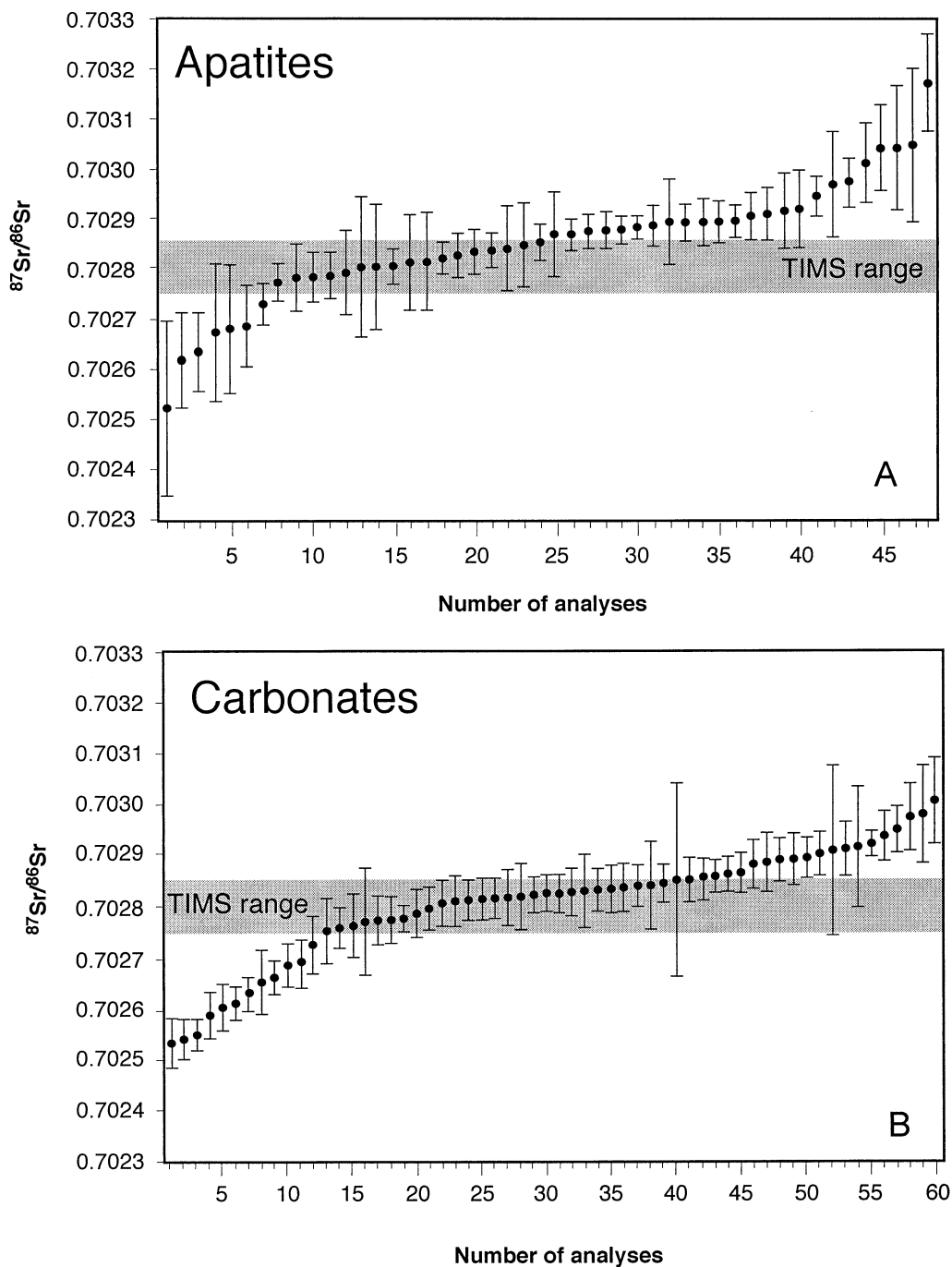


Fig. 7. Diagram showing range of $^{87}\text{Sr}/^{86}\text{Sr}$ values obtained for (A) apatites and (B) carbonates from sample SARF-10. Gray area depicts range of $^{87}\text{Sr}/^{86}\text{Sr}$ values obtained for whole-rock thermal ionization mass spectrometry (TIMS) analyses from sample SARF-10. Error bars represent uncertainties at 2σ level. Data are from Table 3.

throughout the solidification history of the sample. Experimental studies have demonstrated that apatite and carbonate may represent simultaneous liquidus phases over a wide range of pressures and temperatures (e.g., Wyllie et al., 1962; Biggar, 1969; Hoggart, 1989). This is in accordance with the petrographic features of the studied samples because both apatite and carbonate crystals occur as cumulus and intercumulus phases. As such, both minerals can potentially monitor the

isotopic evolution of the melt during crystallization. The range of $^{87}\text{Sr}/^{86}\text{Sr}$ values in apatites and carbonates is consistent with mixing of distinct generations of crystals cognate to a melt undergoing progressive change in isotopic composition. This may be achieved by melting under open-system conditions, resulting in mixing of components (melts, fluids) with different $^{87}\text{Sr}/^{86}\text{Sr}$ isotopic ratios. The spread of data may thus be reconciled with either (1) a melt with a high initial $^{87}\text{Sr}/^{86}\text{Sr}$

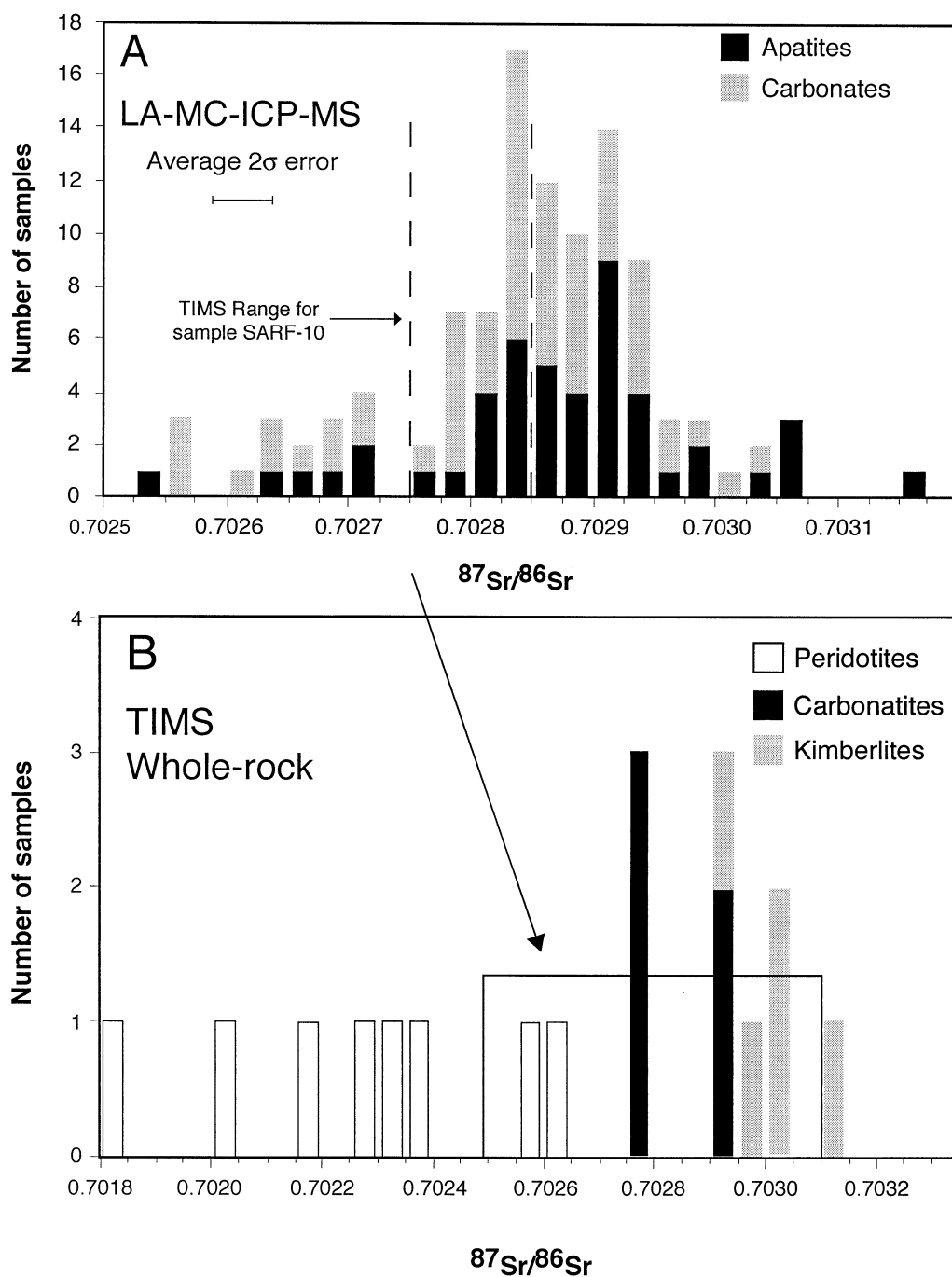


Fig. 8. Histograms showing variations of Sr isotopic compositions for different rock types and minerals of the Sarfartoq alkaline province of Greenland. (A) Range of $^{87}\text{Sr}/^{86}\text{Sr}$ values obtained by laser-ablation multicollector inductively coupled plasma mass spectrometry (LA-MC-ICP-MS) for apatites and carbonates from sample SARF-10. Data from Table 3. (B) Range of $^{87}\text{Sr}/^{86}\text{Sr}$ values obtained by thermal ionization mass spectrometry (TIMS) for whole-rock analyses of kimberlites, carbonatites, and kimberlite-hosted peridotites from Sarfartoq complex. Box represents range of values obtained by LA-MC-ICP-MS. TIMS data from Bizzarro and Stevenson (unpublished data).

undergoing progressive exchange with a less radiogenic component or (2) an initial melt with a low Sr isotopic composition evolving toward high $^{87}\text{Sr}/^{86}\text{Sr}$ values. As discussed earlier, lower Sr isotopic compositions have been recorded by large carbonate crystals associated with oxide (magnetite) segrega-

tions. The core-rim variations observed in phlogopite crystals present as inclusions in the carbonate with lower isotopic compositions suggest that these precipitated during later stages of the crystallization history of the magma. Therefore, the isotopic composition recorded by the carbonate crystals in

Table 5. Major element variation among single phlogopite crystals.

	Na ₂ O	F	K ₂ O	FeO	SiO ₂	MgO	TiO ₂	CaO	MnO	Al ₂ O ₃	Total
Phlogopite 1											
Core	0.41	0.48	10.41	9.06	41.13	24.63	0.32	0.06	0.05	9.81	96.35
Rim	0.15	0.82	10.17	14.66	40.33	22.34	0.18	0.35	0.08	7.28	96.34
Phlogopite 2											
Core	0.27	0.46	10.45	10.04	41.29	24.38	0.18	0.02	0.05	9.21	96.35
Rim	0.13	0.45	10.55	13.99	40.30	21.86	0.07	0.15	0.06	8.43	95.98
Rim	0.09	0.76	10.66	14.39	40.10	21.92	0.14	0.17	0.04	8.19	96.46
Rim	0.22	0.52	10.57	11.24	40.63	24.07	0.18	0.15	0.06	8.51	96.16
Phlogopite 3											
Core	0.30	0.48	10.02	10.64	40.97	24.31	0.24	0.21	0.04	8.73	95.92
Core	0.29	0.61	10.08	10.53	40.90	23.91	0.21	0.22	0.04	8.99	95.78
Rim	0.18	1.14	10.24	11.29	40.28	23.82	0.21	0.44	0.05	8.72	96.36
Rim	0.20	0.84	10.10	12.43	40.52	23.36	0.16	0.34	0.06	8.22	96.22

Analyses reported in weight percentage. Grains selected for analyses were small (< 1 mm) inclusions found in carbonates associated with magnetite (e.g., Fig. 2A).

which phlogopite inclusions with tetraferriphlogopite rims occur may represent the isotopic composition of the melt during a later stage of the crystallization sequence, whereas other carbonate crystals may record secular isotopic changes experienced by the melt upon initial melting. In this respect, it is possible that the range of $^{87}\text{Sr}/^{86}\text{Sr}$ recorded by the large carbonate and apatite crystals may be explained by crystal fractionation from a melt of initially high $^{87}\text{Sr}/^{86}\text{Sr}$ composition undergoing isotopic exchange with a low- $^{87}\text{Sr}/^{86}\text{Sr}$ component. The correlation observed between isotopic composition and texture within carbonate crystals supports episodic melt replenishment, and the isotopic composition of the fine-grained carbonate crystals may thus represent the isotopic nature of a scavenging melt.

4.2. Mantle Sources

The isotopic signatures of mantle components most likely involved in the genesis of the carbonatite complex at Sarfartoq, i.e., plume material and subcontinental mantle (SCM), have been characterized through the study of peridotite xenoliths and host kimberlites (Bizzarro and Stevenson, unpublished data). Peridotite xenoliths yield an average Sr isotopic composition of 0.70225 ± 27 (2σ , $n = 8$), whereas the kimberlites, possible derivatives of the plume component, have an average whole-rock $^{87}\text{Sr}/^{86}\text{Sr}$ ratio of 0.70297 ± 6 (2σ , $n = 5$). In addition, a number of carbonatite samples from the Sarfartoq alkaline complex yield an average whole-rock $^{87}\text{Sr}/^{86}\text{Sr}$ ratio of 0.70276 ± 8 (2σ , $n = 4$). The whole-rock data clearly indicate that the carbonatites at Sarfartoq may not have been generated by melting of SCM but necessitate the involvement of a more radiogenic component, such as plume material (Fig. 8B). The range in $^{87}\text{Sr}/^{86}\text{Sr}$ ratios recorded by apatites and carbonates (0.7025 to 0.7031) overlaps the isotopic compositions of kimberlites, carbonatites, and peridotite xenoliths at Sarfartoq. This indicates that the observed spread of Sr isotopic compositions may be generated by the mixing of at least two end-members, represented by kimberlites and peridotites (i.e., plume and lithosphere), respectively. Thus, the Sr isotope compositions for the apatite and carbonate crystals can represent a record of temporal evolution of a plume-derived magma undergoing isotopic exchange with the overlying SCM reservoir. It is possible

that the Sr isotopic variations defined by apatite and carbonate at the scale of individual hand specimens are a reflection of larger (regional) scale open-system processes involving mixing of distinct mantle sources, which include SCM and upwelling plume material. Alternatively, Bell and Tilton (2001) have recently proposed carbonatite generation via plumes originating from the deep mantle (bottom 1000 km) involving the HIMU and EM1 mantle components. The HIMU-EM1 mixing trends observed in African carbonatites do not reflect interaction of a plume (HIMU) component with enriched lithosphere (EM1) but stem from the isotopic heterogeneity of the plume source itself (Bell and Tilton, 2001). The variation in $^{87}\text{Sr}/^{86}\text{Sr}$ compositions documented in this study may therefore also be explained by isotopic heterogeneity inherent to the plume source.

5. CONCLUSIONS

This study is the first to report $^{87}\text{Sr}/^{86}\text{Sr}$ compositions for coexisting igneous minerals (carbonate and apatite) from the same $\sim 50\text{-}\mu\text{m}$ -thick section. On the basis of the results presented here, the LA-MC-ICP-MS method provides a rapid and effective approach to determine the extent of isotopic heterogeneity within a single sample or individual grains, with analytical precision approaching that obtained by TIMS. This study reveals the importance of detailed, in situ isotopic work for deciphering the complex dynamics of magmatic systems. The LA data obtained here reveal a somewhat complicated petrogenetic history for the Sarfartoq carbonatite complex, involving crystal fractionation under open-system conditions with possible interaction of different mantle reservoirs. The range of $^{87}\text{Sr}/^{86}\text{Sr}$ values recorded by apatite and carbonate indicate that the melt was undergoing progressive isotopic exchange throughout its crystallization history. Compared to the whole-rock Sr isotopic compositions for associated kimberlites, carbonatites, and mantle-derived peridotites (obtained by TIMS), the LA data obtained here may be attributed to the interaction of plume and SCM reservoirs that took place during generation of the carbonatite at Sarfartoq. Alternatively, the observed isotopic variations may reflect isotopic heterogeneity within a plume mantle source (Bell and Tilton, 2001).

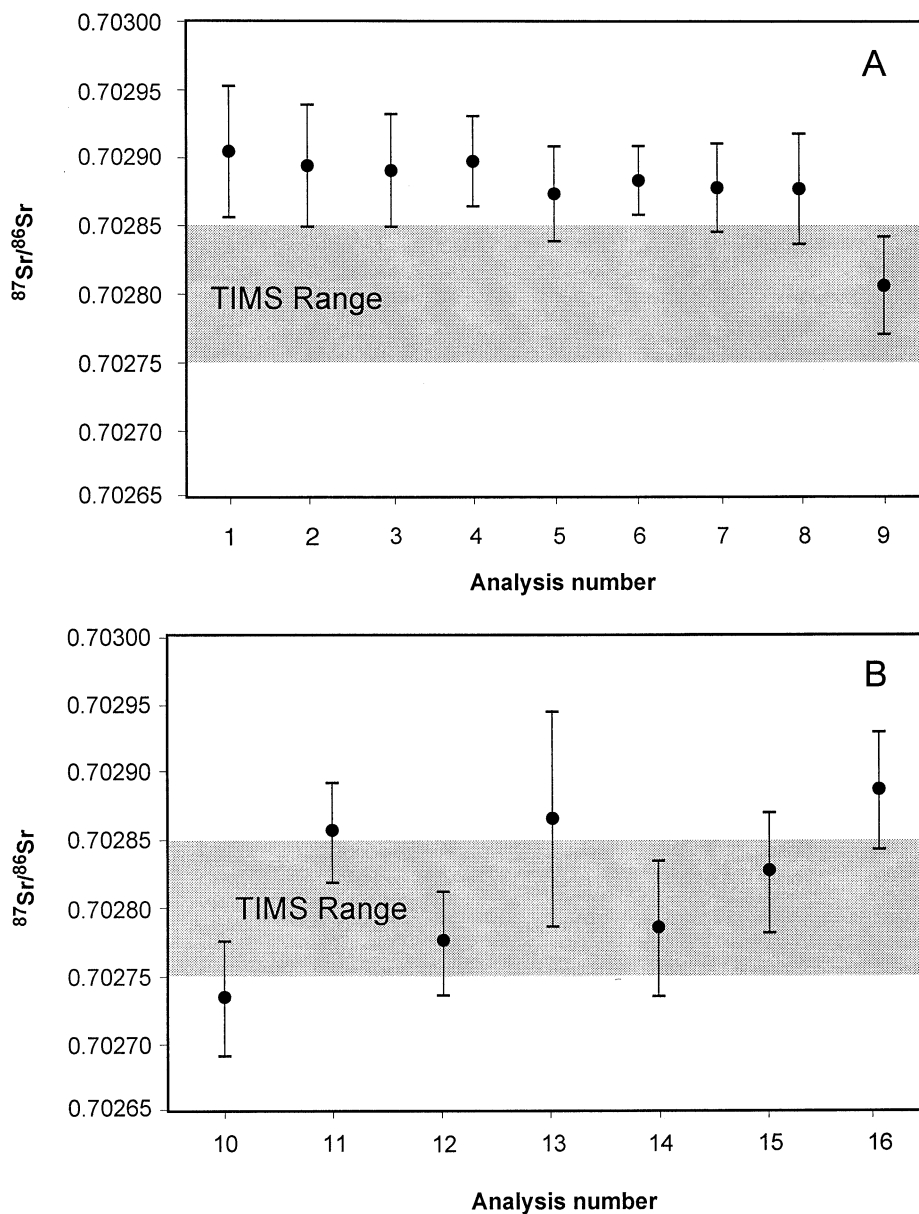


Fig. 9. Diagrams showing intramineral variations of the $^{87}\text{Sr}/^{86}\text{Sr}$ composition in two different apatite crystals from sample SARF-10. Gray area depicts range of $^{87}\text{Sr}/^{86}\text{Sr}$ values obtained for whole-rock thermal ionization mass spectrometry (TIMS) analyses from sample SARF-10. Error bars represent uncertainties at 2σ level. Analysis numbers correspond to those listed in Table 3. (A) Measurements taken across a section perpendicular to the long axis of a euhedral grain. Section is 3.5 mm wide. (B) Measurements taken along the length of a 5.5-mm by 1.5-mm wide anhedral crystal.

Acknowledgments—Financial support for this project was provided through a Natural Sciences and Engineering Research Council of Canada grant to R. K. Stevenson. Martin Bizzarro acknowledges the Fonds pour la Formation de Chercheurs et l'aide à la Recherche Bourse de Recherche en Milieu Pratique program for a Ph.D. scholarship. De Beers Canada Exploration Inc. is thanked for support during fieldwork. Glenn Poirier and Glenna Keating (both at McGill University, Montréal, Canada) are thanked for help with the microprobe and XRF analyses, respectively. Reviews by Andrew Campbell and two anonymous reviewers improved the quality of this manuscript.

Associate editor: R. J. Walker

REFERENCES

- Bell K. (1998) Radiogenic isotope constraints on relationships between carbonatite and associated silicate rocks—A brief review. *J. Petrol.* **39**, 1987–1996.
- Bell K. and Simonetti A. (1996) Carbonatite magmatism and plume activity: Implications from the Nd, Pb and Sr isotope systematics of Oldoinyo Lengai. *J. Petrol.* **37**, 1321–1329.
- Bell K. and Tilton G. R. (2001) Nd, Pb and Sr isotopic compositions of East African carbonatites: Evidence for mantle mixing and plume inhomogeneity. *J. Petrol.* **42**, 1927–1945.
- Biggar G. M. (1969) Phase relationships in the join $\text{Ca}(\text{OH})_2\text{-CaCO}_3\text{-Ca}_3\text{PO}_4\text{-H}_2\text{O}$ at 1000 bars. *Mineral. Mag.* **37**, 75–82.

- Bizzarro M., Simonetti A., Stevenson R. K., and David J. (in press) Hf isotope evidence for a hidden mantle reservoir. *Geology*, **30**, 771–774.
- Christensen J. N., Halliday A. N., Lee D.-C., and Hall C. M. (1995) In situ Sr isotopic analysis by laser ablation. *Earth Planet. Sci. Lett.* **136**, 79–85.
- Colonna M. (1994) *Chronologie des variations du niveau marin au cours du dernier cycle climatique. (0-140 000 ans) dans la partie occidentale de l'océan Indien*. Ph.D. dissertation, Université de Provence, France.
- Davidson J. P. and Tepley F. J. III (1997) Recharge in volcanic systems; evidence from isotopic profiles of phenocrysts. *Science* **275**, 826–829.
- Davidson J., Tepley F. III, Palacz Z., and Meffan-Main S. (2001) Magma recharge, contamination and residence times revealed by in situ laser ablation isotopic analysis of feldspar in volcanic rocks. *Earth Planet. Sci. Lett.* **184**, 427–442.
- Eggins S. M., Kinsley L. P. J., and Shelley J. M. G. (1998) Deposition and element fractionation processes during atmospheric pressure sampling for analysis by ICP-MS. *Appl. Surf. Sci.* **127–129**, 278–286.
- Hoggart D. D. (1989) Pyrochlore, apatite and amphibole: Distinctive minerals in carbonatites. In *Carbonatites, Genesis and Evolution* (ed. K. Bell), pp. 105–148. Allen and Unwin, London.
- Horn I., Rudnick R. L., and McDonough W. F. (2000) Precise elemental and isotope ratio determination by simultaneous solution nebulization and laser ablation-ICP-MS: Application to U-Pb geochronology. *Chem. Geol.* **164**, 281–301.
- Jackson S. E., Pearson N. J., Griffin W. L. (2001) In situ isotope ratio determination using laser-ablation (LA)-magnetic sector-ICP-MS. In *Laser-Ablation-ICP-MS in the Earth Sciences* (ed. P.J. Sylvester), Mineralogical Association of Canada short course series, **29**, 105–119.
- Kalsbeek F., Pidgeon R. T., and Taylor P. N. (1987) Nagssugtoqidian mobile belt of West Greenland: A cryptic 1850 Ma suture between two Archaean continents—chemical and isotopic evidence. *Earth Planet. Sci. Lett.* **85**, 385–395.
- Kalsbeek F. and Nutman A. P. (1996) Anatomy of the Early Proterozoic Nagssugtoqidian orogen, West Greenland, explored by reconnaissance SHRIMP U-Pb dating. *Geology* **24**, 515–518.
- Larsen L. M. and Rex D. C. (1992) A review of the 2500 Ma span of alkaline-ultramafic, potassic and carbonatitic magmatism in West Greenland. *Lithos* **28**, 367–402.
- McCormick G. R. and Le Bas M. J. (1996) Phlogopite crystallization in carbonatitic magmas from Uganda. *Can. Mineral.* **34**, 469–478.
- Russell W. A., Papanastassiou D. A., and Tombrello T. A. (1978) Ca isotope fractionation on the Earth and other solar system materials. *Geochim. Cosmochim. Acta* **42**, 1075–1090.
- Secher K. and Larsen L. M. (1980) Geology and mineralogy of the Sarfartoq carbonatite complex, southern West Greenland. *Lithos* **13**, 199–212.
- Simonetti A., Goldstein S. L., Schmidberger S. S., and Viladkar S. G. (1998) Geochemical and Nd, Pb, and Sr isotope data from Deccan alkaline complexes—Inferences for mantle sources and plume-lithosphere interaction. *J. Petrol.* **39**, 1847–1864.
- Wallace M. E. and Green D. H. (1988) An experimental determination of primary carbonatite magma composition. *Nature* **335**, 343–346.
- Wyllie P. J., Cox K. G., and Biggar G. M. (1962) The habits of apatite in synthetic systems and igneous rocks. *J. Petrol.* **3**, 238–243.